An Evaluation of the Use of Atmospheric and BRDF Correction to Standardize Landsat Data

Fuqin Li, *Senior Member, IEEE*, David L. B. Jupp, Shanti Reddy, Leo Lymburner, Norman Mueller, Peter Tan, and Anisul Islam

***Abstract*—Normalizing for atmospheric and land surface bidirectional reflectance distribution function (BRDF) effects is essential in satellite data processing. It is important both for a single scene when the combination of land covers, sun, and view angles create anisotropy and for multiple scenes in which the sun angle changes. As a consequence, it is important for inter-sensor calibration and comparison. Procedures based on physics-based models have been applied successfully with the Moderate Resolution Imaging Spectroradiometer (MODIS) data. For Landsat and other higher resolution data, similar options exist. However, the estimation of BRDF models using internal fitting is not available due to the smaller variation of view and solar angles and infrequent revisits. In this paper, we explore the potential for developing operational procedures to correct Landsat data using coupled physics-based atmospheric and BRDF models. The process was realized using BRDF shape functions derived from MODIS with the MODTRAN 4 radiative transfer model. The atmospheric and BRDF correction algorithm was tested for reflectance factor estimation using Landsat data for two sites with different land covers in Australia. The Landsat reflectance values had a good agreement with ground based spectroradiometer measurements. In addition, overlapping images from adjacent paths in Queensland, Australia, were also used to validate the BRDF correction. The results clearly show that the algorithm can remove most of the BRDF effect without empirical adjustment. The comparison between normalized Landsat and MODIS reflectance factor also shows a good relationship, indicating that cross calibration between the two sensors is achievable.**

***Index Terms*—Atmospheric correction, bidirectional reflectance distribution function, Landsat and Moderate Resolution Imaging Spectroradiometer (MODIS).**

I. Introduction

LANDSAT imagery has been used extensively for terrestrial environment assessment and natural resources inventory for decades ([1]–[3]). In recent times, a range of data types of similar resolution to Landsat, such as Indian Remote Sensing Resourcesat (IRS-P6) and Advanced Land Observing Satellite (ALOS), have also become routinely acquired in Australia. It is widely recognized that the raw remotely sensed data received by these satellites in the solar spectral range do not directly characterize the underlying reflectance of surface objects since, even for the same surface type, the received radiance at the satellite is different due to the variations of atmospheric properties, and solar zenith, azimuth and sensor view angles. Many of the effects of the atmosphere on the signal can be overcome by a general scaling or atmospheric correction to the data. However, for given atmosphere and land surface there are also variations with sun and sensor geometry which will be referred to here generally as the Multi-Sun and View Angle (MSVA) effect. Part of the effect occurs in the atmosphere and part is a function of the land cover type and its condition. The latter has had special attention in recent years and is usually referred to as land surface Bidirectional Reflectance Distribution Function (BRDF). The specific definition of BRDF was developed as a property of materials that is not modified by the incident radiation in [4] and was used there to derive a range of standard types of reflectance factors for materials as a function of source and view geometry. The terms "BRDF" and "BRDF effect" in this paper refer to this underlying property and where the values of specific types of reflectance factor (such as BRF or bi-directional reflectance factor which is π times the BRDF) are used we have made use of recent reviews of terminology by [5], [6] to indicate reflectance factor type. More details about the general topic of BRDF can be accessed in the collection of papers edited by Liang and Strahler in [7], but it is important to mention that we have adopted the "statistical" formulation of BRDF more recently developed by [8] and [9].

To obtain consistent and comparable measures of surface reflectance from remote sensing observations it is necessary to process the data to reduce or remove these effects. The retrieved surface reflectance can then be used to measure land surface change through a time series or characterize land cover in a way that does not need to be tailored to each image. The atmospheric and BRDF correction is also essential to conduct field validation and to allow various sensors and satellite systems to be directly compared for specific surface covers. One option is to use physically based atmospheric and BRDF correction. However, while theory for physics-based correction has been known for many years, there have been some practical impediments to adopting it, such as choice of BRDF model, data for atmospheric profile (water vapour) and aerosol information etc. Consequently, many empirical, data dependent and exploratory methods have been adopted. These methods have often been used successfully (e.g., [10] and [11]), but the results have not always been consistent due to different landscapes and environment for the

Manuscript received June 16, 2009; revised November 10, 2009. Date of publication March 01, 2010; date of current version August 25, 2010. This work was supported in part by Geoscience Australia and in part by CSIRO for ongoing Landcover and Terrestrial and Ecosystem Research Network projects.

F. Li, L. Lymburner, N. Mueller, P. Tan, and A. Islam are with the National Earth Observation Group, Geoscience Australia, ACT, 2601, Australia (e-mail: fuqin.li@ga.gov.au; leo.lymburner@ga.gov.au; norman.mueller@ga.gov.au; peter.tan@ga.gov.au; anisul.islam@ga.gov.au).

D. L. B. Jupp is with CSIRO, Marine and Atmospheric Research, ACT 2601, Australia (e-mail: david.jupp@csiro.au).

S. Reddy is with the Land Management Branch, Department of Climate Change, ACT 2601, Australia (e-mail: shanti.reddy@climatechange.gov.au).

Color versions of one or more of the figures in this paper are available online at http://ieeexplore.ieee.org.

Digital Object Identifier 10.1109/JSTARS.2010.2042281

study areas and success is often a function of available data and the experience of the researchers. Empirical normalization does not in general lead to estimates of true and objectively defined surface reflectance, presenting difficulties for validation and between-sensor comparisons which must rely on broad, data dependent statistical correlations. As a result of this, it has not been easy to apply empirical methods in a consistent way to new areas, countries or to different sensors.

As indicated before, physically based models can be used to overcome the above problem, but they face a number of difficulties. One is the need to establish specific parameters for the model, such as vertical profiles of atmosphere, aerosol type and amount and also BRDF parameters. A model for surface BRDF in particular cannot be independently derived from Landsat data and separated from atmospheric effects due to the small variation of relative view and solar angles, consistent sun-synchronous view of a given location and infrequent revisit period of the sensor. Instead, one must use BRDF information from another source. A pointer to the possible way to do this has been provided from **POL**arization and **D**irectionality of the **E**arth's **R**eflectances (POLDER) data from which [12] found that Bidirectional Anisotropy Standard shapE (BASE, a normalized BRDF function equivalent to the shape function used later in this paper) was very similar within and distinct between different vegetation types. If relationships such as they found persist for land covers and regions and with the development global MODIS BRDF model products [13], it may be possible to conduct atmospheric and BRDF correction for Landsat data using a physically based model in a consistent way in every country. Because MODIS has a wide range of sun and view angles and the data can be acquired daily, the sensor has also been used to measure and monitor BRDF properties globally. This in turn has enabled the BRDF correction of MODIS data through internal adjustment. At this time, continuing 16 days composite MODIS BRDF model parameters with 500 m resolution are available online to the public at global scale ([13], https://wist.echo.nasa.gov/api). In this paper, we explore use of the MODIS BRDF model shape function and MODTRAN 4 radiative transfer model to conduct BRDF and atmospheric correction for Landsat data using a coupled BRDF and atmospheric correction model.

II. Methods Selected for the Study

A. Basic Theory

Since the components of the algorithms need to be collated from a number of sources, it is useful to briefly summarize the combined set of equations used in the physical correction. According to [14]–[17], an expression for the reflectance at the top of atmosphere (the TOA reflectance factor) for a nonuniform surface can be written in the form

$$\rho_{TOA} = \rho_0 + t_V t_S \rho_s(\theta_S, \theta_V, \varphi) + t_V t_d(\theta_S)\overline{\rho} + t_S t_d(\theta_V)\overline{\rho'} + t_d(\theta_S)t_d(\theta_V)\overline{\overline{\rho}} + \frac{[t_V + t_d(\theta_V)][t_S + t_d(\theta_S)]S(\overline{\overline{\rho}})^2}{1 - S\overline{\overline{\rho}}}. \quad (1)$$

In this expression, ρ_{TOA} is the measurable reflectance at top of atmosphere (π times measured exiting radiance within the IFOV of the sensor, which is assumed to be small, divided by the solar irradiance), ρ_0 is the intrinsic atmospheric reflectance (path reflectance) due to returning radiation that does not interact with the surface. $\rho_s(\theta_S, \theta_V, \varphi)$ is the surface reflectance (the BRF), θ_S is solar zenith angle and θ_V is view zenith angle, φ is relative azimuth between the sun and view directions. t_S and t_V are direct transmittance in the solar and view directions. $t_d(\theta_S)$ and $t_d(\theta_V)$ are diffuse transmittance in the solar and view directions; $\overline{\rho}$, $\overline{\rho'}$, and $\overline{\overline{\rho}}$ are surface hemispherical-directional, directional-hemispherical and hemispherical-hemispherical reflectance (or bi-hemispherical) factors, respectively, and S is atmospheric albedo which is the bi-hemispherical ratio between upwelling radiation from the surface and the downwelling radiation

This expression is an approximation for the solution for the exiting radiance obtained by radiative transfer modeling with the above normalization to reflectance factors but effective values for the parameters ρ_0, t_S, t_V, $t_d(\theta_S)$, $t_d(\theta_V)$, and S can be identified using radiative transfer modeling (e.g., MODTRAN4 or 6S) runs in a way that makes (1) an accurate approximation. The formulation can also provide the means to derive various levels of correction and standard products. For example, if the land surface has no multiview angle (BRDF) effect (i.e., it is a Lambertian surface) and we also assume that the region around a pixel is a similar land cover type as the pixel in question with reflectance ρ_t then (1) simplifies to

$$\rho_{TOA} = \rho_0 + T_V T_S \frac{\rho_t}{1 - S\rho_t}. \quad (2)$$

In this expression, $T_S = t_S + t_d(\theta_S)$ and $T_V = t_V + t_d(\theta_V)$ are the total atmospheric transmittances corresponding to the sun and view directions. If radiative transfer code is used to identify these terms (2) can be inverted and leads to a first estimate for surface reflectance as the solution to the equation

$$\frac{\rho_{TOA} - \rho_0}{T_V T_S} = \frac{\rho_m}{1 - S\rho_m} \quad (3)$$

where ρ_m is the atmospherically corrected Lambertian reflectance or, if the input data does not satisfy the assumptions, a first estimate for the surface reflectance which we will refer to as the "Lambertian" reflectance (i.e., the reflectance obtained assuming the surface is Lambertian).

If one also assumes that for Landsat data the view angle variation is negligible and that the solar angle changes very little then (3) can be applied at every pixel. This is how Landsat data have often been atmospherically corrected in the past. In the examples to follow this is called correction using coefficients at the center point since it is usual to use the sun position at the center point and assume that $\theta_V \approx 0$ over the whole image. However, we know that between and within scenes, the sun and view angles can vary to create significant atmospheric effects and that the land surface multiview angle component due to BRDF increases the total MSVA effect. Our objective is to normalize these remaining effects to standard sun and nadir view angles for all images in a time series and consistently between different locations.

A practical approach to handling BRDF that has become well established during the development of MODIS products is to use kernel models ([18], [19]). In this approach, $\rho_s(\theta_S, \theta_V, \varphi)$ (the

BRF) can be semi-empirically expressed using kernel functions in the form

$$\rho_s(\theta_S, \theta_V, \varphi) = F_{iso} + F_{vol}K_{vol} + F_{geo}K_{geo} \tag{4}$$

where F_{iso} is the isotropic contribution. F_{vol} and F_{geo} are the weights for volume-scattering and geometric-optical contributions and K_{vol} and K_{geo} are volume-scattering and geometrical-optical scatting kernel functions. K_{vol} and K_{geo} are defined functions of θ_S, θ_V and φ. Changing the form of (4) and defining that $\alpha 1 = F_{vol}/F_{iso}$ and $\alpha 2 = F_{geo}/F_{iso}$ then

$$\begin{aligned}\rho_s(\theta_S, \theta_V, \varphi) &= F_{iso}\left(1 + \frac{F_{vol}}{F_{iso}}K_{vol} + \frac{F_{geo}}{F_{iso}}K_{geo}\right)\\ &= F_{iso}B(\theta_S, \theta_V, \varphi, \alpha 1, \alpha 2).\end{aligned} \tag{5}$$

The term $B(\theta_S, \theta_V, \varphi, \alpha 1, \alpha 2)$ will be called the BRDF shape function (equivalent to the BASE defined by [12]) and is a function of solar, view and azimuth angles as well as $\alpha 1$ and $\alpha 2$. For a special case when $\theta_s = \theta_v = 0$, it follows that $B = 1$.

It is the shape function rather than the complete BRF that is needed to resolve the angle effects. From the work of the MODIS science team [19], [20], if it is assumed that the kernel model is valid and all purely diffuse radiation has a uniform angular distribution, then the reflectance factors $\overline{\rho}$, $\overline{\rho'}$ and $\overline{\overline{\rho}}$ (called black sky and white sky albedos in this case by the MODIS science team) can be closely estimated by polynomial approximation as

$$\begin{aligned}\overline{\rho} &= F_{iso}[1 + \alpha 1(-0.007574 - 0.070987{\theta_V}^2 + 0.307588{\theta_V}^3)\\ &\quad + \alpha 2(-1.284909 - 0.166314{\theta_V}^2 + 0.041840{\theta_V}^3)]\\ &= F_{iso}\alpha_{bk}(1, \alpha 1, \alpha 2, \theta_V).\end{aligned} \tag{6}$$

Similarly with (6) since the kernels are assumed to be reciprocal and there is no environmental effect

$$\overline{\rho'} = F_{iso}\alpha_{bk}(1, \alpha 1, \alpha 2, \theta_S). \tag{7}$$

The white sky albedo (a bi-hemispherical reflectance factor) $\overline{\overline{\rho}}$ can be expressed as

$$\begin{aligned}\overline{\overline{\rho}} &= F_{iso}(1 + 0.189184\alpha 1 - 1.377622\alpha 2)\\ &= F_{iso}\alpha_{wk}(1, \alpha 1, \alpha 2).\end{aligned} \tag{8}$$

Combining (5)–(8) with (1) and defining $f_V = t_V/T_V$ and $f_S = t_S/T_S$ and $F_{iso} = \overline{\overline{\rho}}/\alpha_{wk}(1, \alpha 1, \alpha 2)$, it follows that

$$\begin{aligned}\rho_{TOA} &= \rho_o + f_V f_S T_V T_S \frac{\overline{\overline{\rho}}}{\alpha_{wk}(1, \alpha 1, \alpha 2)} B(\theta_S, \theta_V, \varphi, \alpha 1, \alpha 2)\\ &\quad + f_V(1 - f_S)T_V T_S \frac{\overline{\overline{\rho}}}{\alpha_{wk}(1, \alpha 1, \alpha 2)}\alpha_{bk}(1, \alpha 1, \alpha 2, \theta_V)\\ &\quad + f_S(1 - f_V)T_V T_S \frac{\overline{\overline{\rho}}}{\alpha_{wk}(1, \alpha 1, \alpha 2)}\alpha_{bk}(1, \alpha 1, \alpha 2, \theta_S)\\ &\quad + (1 - f_S)(1 - f_V)T_V T_S \overline{\overline{\rho}} + \frac{T_V T_S S(\overline{\rho})^2}{1 - S\overline{\overline{\rho}}}.\end{aligned} \tag{9}$$

Combining (3) with (9), we find

$$\begin{aligned}\frac{\rho_m}{1 - S\rho_m} &= f_V f_S \frac{\overline{\overline{\rho}}}{\alpha_{wk}(1, \alpha 1, \alpha 2)} B(\theta_S, \theta_V, \varphi, \alpha 1, \alpha 2)\\ &\quad + f_V(1 - f_S)\frac{\overline{\overline{\rho}}}{\alpha_{wk}(1, \alpha 1, \alpha 2)}\alpha_{bk}(1, \alpha 1, \alpha 2, \theta_V)\\ &\quad + f_S(1 - f_V)\frac{\overline{\overline{\rho}}}{\alpha_{wk}(1, \alpha 1, \alpha 2)}\alpha_{bk}(1, \alpha 1, \alpha 2, \theta_S)\\ &\quad + (1 - f_S)(1 - f_V)\overline{\overline{\rho}} + \frac{S(\overline{\rho})^2}{1 - S\overline{\overline{\rho}}}\\ &= a\overline{\overline{\rho}} + \frac{S(\overline{\rho})^2}{1 - S\overline{\overline{\rho}}}\end{aligned} \tag{10}$$

where (see the equation shown at the bottom of the page).

With some manipulation, this reduces to

$$(1 - a)S(1 - S\rho_m)\overline{\overline{\rho}}^2 + [a + \rho_m(1 - a)S]\overline{\overline{\rho}} - \rho_m = 0. \tag{11}$$

It is straightforward to solve the quadratic (11) to get $\overline{\overline{\rho}}$ from the initial estimate ρ_m, and then derive a parameter such as F_{iso} or some form of reflectance factor (such as BRF) normalized to a standard choice of sun and view angles on a pixel by pixel basis.

B. Algorithm Implementation

Provided the Landsat data are calibrated to radiance, atmospheric components, S, T_V, T_S, f_V, f_S, ρ_0 and the atmospherically corrected Lambertian reflectance ρ_m can be obtained using the well-established MODTRAN radiative transfer model with appropriate input data. The input data needed by a radiative transfer model include atmospheric profiles of aerosol, water vapour, CO_2 and ozone along with the acquisition date and time (or day of year and time of day) to obtain sun position as a function of time for the satellite track, plus sensor view and azimuth angles for each pixel. If the BRDF shape function is known at that pixel, then the corrected reflectance can also be obtained and a standardized reflectance output can be generated using the algorithms summarized above.

Since it is time consuming and impractical to run MODTRAN pixel by pixel, some simpler way of estimating the base information is needed if the inputs and parameters can vary within the image and between images. This has been done in MODIS processing by using look-up tables for the parameters that can vary in the image and using look-up tables

$$\begin{aligned}a = {}&1/\alpha_{wk}(1, \alpha 1, \alpha 2)[f_V f_S B(\theta_S, \theta_V, \varphi, \alpha 1, \alpha 2) + f_V(1 - f_S)\alpha_{bk}(1, \alpha 1, \alpha 2, \theta_V)\\ &+ f_S(1 - f_V)\alpha_{bk}(1, \alpha 1, \alpha 2, \theta_S) + (1 - f_S)(1 - f_V)\alpha_{wk}(1, \alpha 1, \alpha 2)].\end{aligned}$$

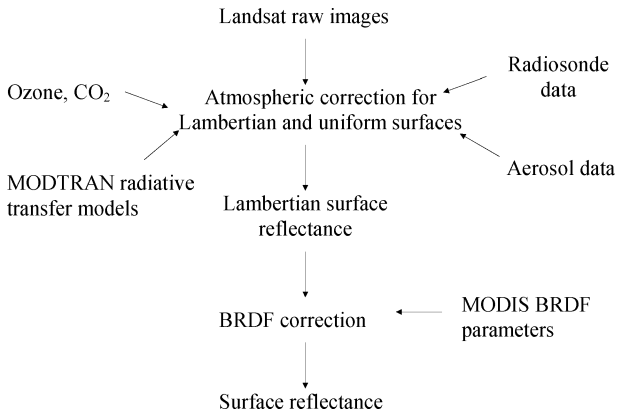

Fig. 1. Diagram for BRDF and atmospheric correction algorithm.

and interpolation of values in the table to estimate atmospheric correction parameters S, T_V, T_S, f_V, f_S, ρ_0, and ρ_m. However, for Landsat and similar resolution images, since the parameters involved vary smoothly and slowly over the image extent, we have used an equivalent but simpler method based on spatial interpolation to reduce the number of MODTRAN runs to a minimum. In this case, MODTRAN runs were made at the corners of a spatial grid to get accurate values for S, T_V, T_S, f_V, f_S, and ρ_0. The values at other points were then obtained by interpolation of the corner values in the regions defined by the grid. It has been found that a quite sparse grid (e.g., of nine corner points) can achieve an accurate result for the extent of a normal Landsat scene. Using this approach, calibrated Landsat images were divided into four rectangles and MODTRAN run at the nine corner coordinates. For any pixel in the image, the MODTRAN outputs are then interpolated from the nine points using bilinear interpolation in each rectangle to get the pixel values. The underlying basis for the effectiveness of the method in this case is the fact that image geometry (pixel and line) can be smoothly transformed to time (identifying location of the sub-satellite point) and off nadir zenith view angle at image pixels. Sun and sensor angles vary smoothly with these parameters. It is, however, convenient and fast to compute the sun and view angles exactly at every pixel.

Fig. 1 outlines the overall work flow for the atmospheric and BRDF correction algorithm. After the MODTRAN outputs for the nine coordinate positions have been obtained and extended to other pixels by interpolation, the Lambertian reflectance (ρ_m) is computed. It is possible for this image to be an intermediate product but in general, if the BRDF shape function is known then (11) can be used to obtain a surface reflectance factor normalized to some specified standard sun and view geometry. The bilinear interpolation method used has made the correction rapid to implement so that a number of different outputs and intermediate images are possible to compare. The algorithm also has the advantage that it does not need to be inserted into existing and well established data processing streams but can be run as a post-process even for schemes that already provide the ρ_m product.

In this study, it has been assumed that the BRDF shape needed is one defined for large regions (regional scale). Finer scale variation in BRDF functions obtained from MODIS, MISR and POLDER have been assumed to be caused by the specific geometry of the local terrain and cover rather than an average statistical regional effect. In this way, local variations due to MODIS sampling and sub-pixel cloud are also reduced. To illustrate the methods in this paper, the regional effect was estimated by averaging the coefficients of the MODIS BRDF model product for the appropriate date over the entire scene. However, for future implementation, it is assumed that stable and characteristic BRDF shape functions will be defined by spatial region or land cover at an appropriate scale for the sensor involved. If available, this can be easily implemented with little increase in algorithm complexity or reduction in speed.

By comparing the MODIS and Landsat response functions (Fig. 2 and Table I), Landsat BRDF model parameters for each band may be identified by using those for the corresponding MODIS band for the same time period and location as the Landsat data. From Fig. 2 and Table I, it is clear that we can associate TM/ETM band 1 with MODIS band 3, TM/ETM band 2 with MODIS band 4, TM/ETM band 3 with MODIS band 1, TM/ETM band 4 with MODIS band 2, TM/ETM band 5 with MODIS band 6 and TM/ETM band 7 with MODIS band 7. Their main differences are due to band FWHM (full width at half maximum, see Fig. 2 and Table I) and the effect of these differences will be further discussed later.

III. Analysis of BRDF Effects for Landsat Data

Due to its small variation in view angle (-7.5° to 7.5°), it is generally accepted that variations due to the BRDF effect are small within a single Landsat scene. It is also commonly assumed (for similar reasons) that it is not necessary to take any account of the MSVA (atmospheric or surface) effect for Landsat images. In most cases, therefore, only "center point" atmospheric correction is conducted, such as in the commercial software FLAASH [21]. However, the MSVA effects of atmosphere are often not negligible and should then be taken into account. In addition, the BRDF effect does produce variations between seasons and geographical regions due to the solar angle variation and for Landsat images with certain common land covers from between the tropics of Capricorn and Cancer surface anisotropy can also become significant for a single scene.

In the following analysis, we will demonstrate how reflectance taking account of the BRDF effect can vary within and between scenes in the eastern part of Australia using parameters of a BRDF model derived from MODIS. Our aim is to see how surface reflectance factor (BRF) will vary along path 91 over the Australian continent (between 23°S in Queensland and 43°S in Tasmania) and between summer and winter due to the multi-angle (sun and view) effect. Four rows (rows 76, 81, 85, and 90) have been used for the analysis. To demonstrate the BRDF effects we can consider a synthetic Landsat 5 path. The surface is taken to be the same non-Lambertian surface in all four scenes and has a nominated BRF value and a specific BRDF shape function (Table II) in each Landsat band. The BRF values and BRDF shape function listed in Table II are based on the average MODIS derived normalized surface reflectance factor (NBAR, or Nadir BRDF-adjusted reflectance) and a BRDF shape function for actual images from path 91 and row 81, i.e., the middle of the "synthetic" Landsat strip. Furthermore

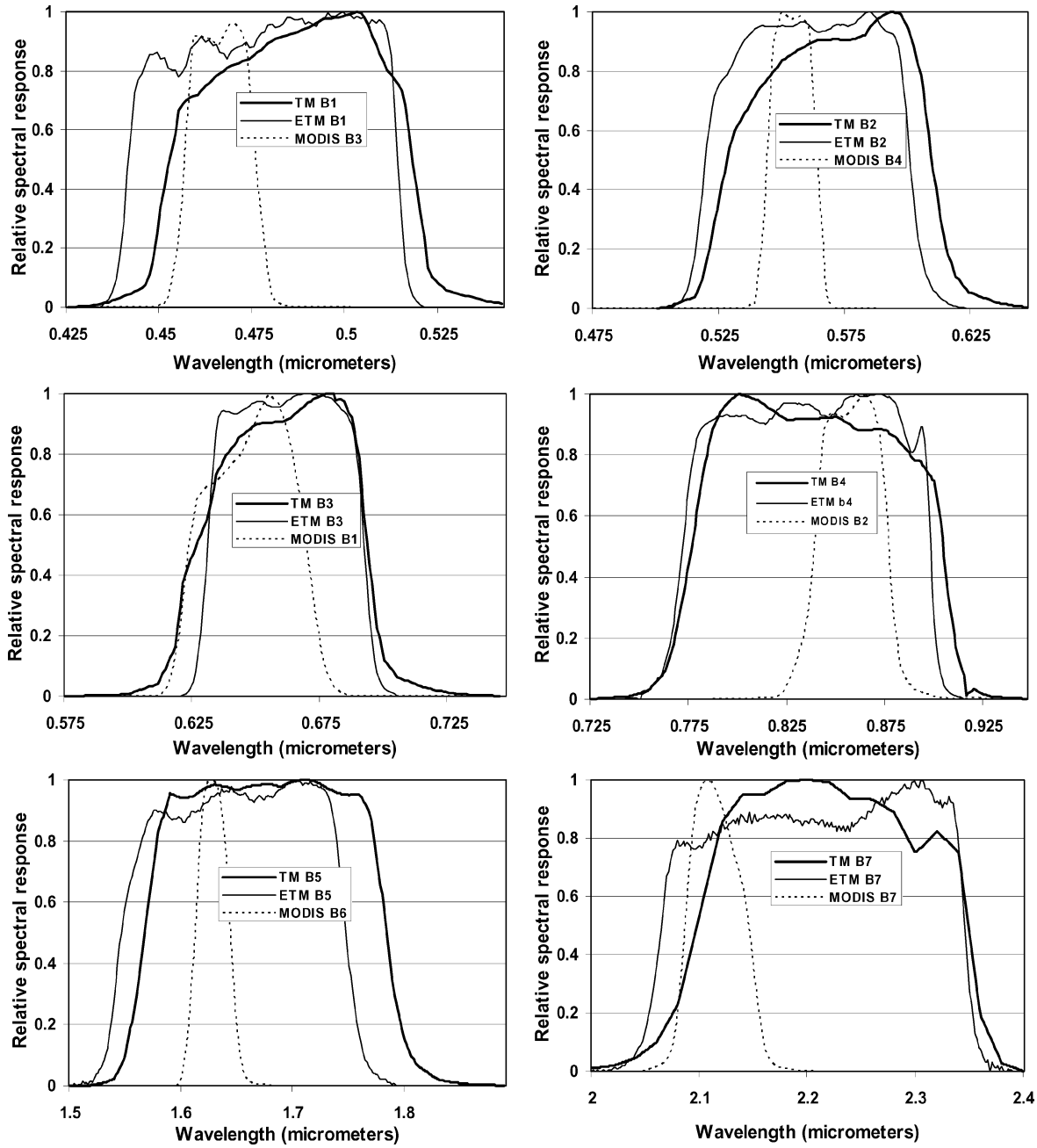

Fig. 2. Comparison between MODIS and Landsat TM relative spectral response.

we have generated a "synthetic" atmosphere with a visibility of 60 km and total water vapour as 1.5 g/cm^3, which is typical Australian atmospheric condition.

With these variables set to fixed values, because all other variables have been constrained, it is possible to assess how the time of year, in this instance described in terms of "Day of year", and latitude influence apparent surface reflectance variations. Table III lists the average latitude and longitude and pass time for the scene center of each of the selected Landsat rows.

Day of year (DOY) 14 (Australian summer) and DOY 190 (Australian winter) are selected for the seasonal analysis. Using the method described in Section II, the BRF values for rows 76, 81, 85, and 90 are plotted in Fig. 3. The figure shows that for a single Landsat scene the BRF varies among 0.005 to 0.030 absolute values between the left and the right edge of the image depending on the seasons if the current BRDF model is used. In summer, when the sun and the satellite close to the principal plane (small relative azimuth angle at the left side of the image), BRF variation within the image is strong being about 10% relative value. The effect is greatest above the Tropic of Capricorn where the Landsat scan lines align closest with the principal plane. In contrast, BRF variation within a single Landsat scene is always small during winter. The BRDF effect is strongest on the western side of the image. This phenomenon can be observed by image display with visual effects indicated by darkening of pixels near the eastern (right) edge and brightening of pixels near western (left) edge of the image. However, compared with within scene variations Fig. 3 shows that BRF varies to a greater

TABLE I
MODIS AND LANDSAT BANDWIDTH AND SPECTRAL RESPONSE FUNCTION

Band	Landsat	B1	B2	B3	B4	B5	B7
	MODIS	B3	B4	B1	B2	B6	B7
Landsat TM	Bandwidth (μm)	0.45-0.52	0.52-0.60	0.63-0.69	0.76-0.90	1.55-1.75	2.08-2.35
	λ_{mean} (μm)	0.486	0.571	0.661	0.838	1.677	2.217
	FWHM	0.061	0.076	0.065	0.120	0.215	0.240
Landsat ETM	Bandwidth (μm)	0.45-0.52	0.53-0.61	0.63-0.69	0.78-0.90	1.55-1.75	2.09-2.35
	λ_{mean} (μm)	0.479	0.561	0.661	0.835	1.650	2.208
	FWHM	0.067	0.078	0.060	0.121	0.190	0.251
MODIS	Bandwidth (μm)	0.46-0.48	0.54-0.57	0.62-0.67	0.84-0.88	1.63-1.65	2.10-2.16
	λ_{mean} (μm)	0.466	0.553	0.648	0.857	1.629	2.115
	FWHM	0.019	0.020	0.040	0.038	0.032	0.056

Note: λ_{mean} is central wavelength for each band.

TABLE II
NOMINATED REFLECTANCE FACTOR (BRF) AND BRDF SHAPE FUNCTION FOR BRDF SEASONAL AND GEOGRAPHICAL ANALYSIS

	B1	B2	B3	B4	B5	B7
F_{iso}	0.0668	0.1086	0.1324	0.2556	0.3302	0.2422
$\alpha 1$	0.3765	0.5287	0.3995	0.7283	0.3361	0.1804
$\alpha 2$	0.2098	0.1952	0.2199	0.1181	0.1913	0.2363

TABLE III
AVERAGE LATITUDE, LONGITUDE AND PASSING TIME FOR PATH 91 IN AUSTRALIAN LAND. SYMBOLS MM IS THE CENTER OF THE IMAGE AND ML AND MR ARE ITS CORRESPONDING LEFT AND RIGHT EDGE OF THE IMAGE, RESPECTIVELY

Row	Centre Time (UTC)	ML		MM		MR	
		Latitude (°S)	Longitude (°E)	Latitude (°S)	Longitude (°E)	Latitude (°S)	Longitude (°E)
76	23.7272	22.9742	150.2961	23.1086	151.2031	23.2376	152.1099
81	23.7606	30.1497	148.4388	30.2942	149.4067	30.4311	150.3744
85	23.7869	35.8682	146.7935	36.0233	147.8275	36.1692	148.8619
90	23.8203	42.9799	144.4411	43.1531	145.5875	43.3142	146.7344

degree between summer and winter. The variation in BRF can reach over 0.08 absolute and 50% relative value for some bands. The four rows show consistent results, particularly for row 90 where the difference between summer and winter is strongest. This is because at high latitudes, the solar angle varies much more between summer and winter.

The BRF variation is governed by the selected shape function. Bands 3 and 7 have the largest geometric component ($\alpha 2$ in Table II). Hence, the BRF variation is largest (Figs. 3 and 4) in these Bands. In practice, therefore, these effects will be greater than shown here for some land covers and less for others.

Fig. 4 is the summary for BRF variation between seasons and geographical regions. In the figure, only the image center (MM) with nadir view is plotted. Therefore, the BRF variation is solely due to the change of solar angle. For band 7 with its strong BRDF effect, the variation in BRF can reach 0.09 absolute value and over 50% relative value between Queensland (row 76) summer and Tasmania (row 90) winter. Both Figs. 3 and 4 show that for Landsat images, the strongest variation due to BRDF effect is from the solar angle change due to seasonal and geographical variation. They also demonstrate how the spectral shape changes due to the varying shape functions between bands. This highlights the importance of applying a BRDF correction to any imagery that will be used for change detection or multitemporal analysis, because BRDF correction is necessary to ensure that changes detected are the result of on-ground changes in biophysical variables rather than due only to changes in sun-sensor geometry.

IV. VALIDATIONS AND COMPARISONS

Section III shows that BRF variation within a Landsat scene, whilst occasionally significant, will more often be small, especially during winter (Fig. 3). However, BRDF correction is important for solar angle normalization for many land covers due to the seasonal and geographical variation. The need to consider the complete time series presents difficulties for designing field experiments that can validate surface BRDF corrections. This is so since most field spectral measurements are conducted at the same time as a satellite overpass and solar and view angles variations are very small within the Landsat scene. Therefore, algorithm validation has been separated into three parts.

1) Validate combined atmospheric and surface BRDF correction using field reflectance measurements.
2) Validate surface BRDF correction using data from image overlap areas of adjacent paths.
3) Cross-validate Landsat data for accuracy of spectral reflectance using the MODIS reflectance product.

A. BRDF and Atmospheric Correction Validation Using Field Data

1) Validation Sites and Reflectance Measurements: Two Australian sites where useful ground data have been taken were used to test the algorithm. One is in the Gwydir area of New South Wales (center location 29.58S, 149.62E). The Gwydir area is covered by forests, crops, grass and bare soil. The second site is at Lake Frome, which is a dry salt lake in

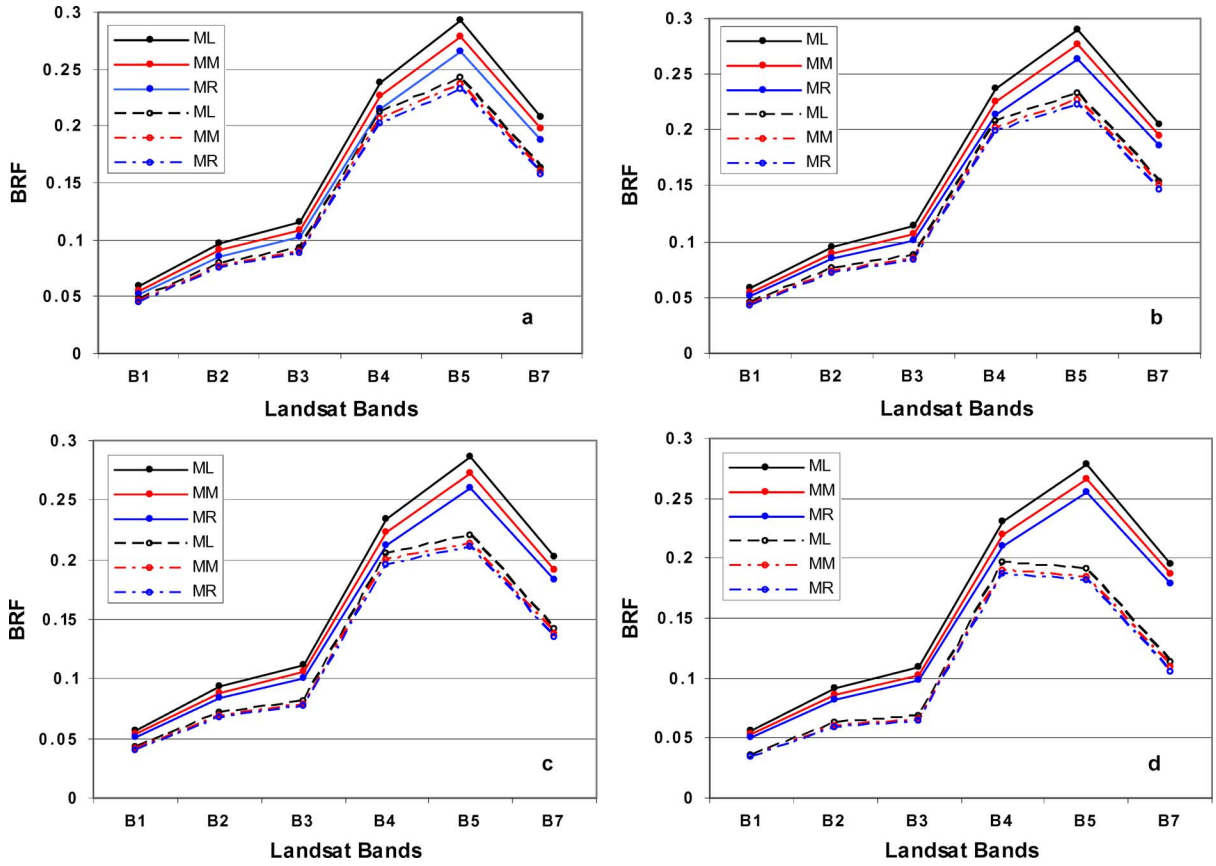

Fig. 3. BRF varies within a single satellite image for (a) row 76, (b) row 81, (c) row 85, and (d) row 90. Symbols MM is the center of the image and ML and MR are its corresponding left and right edge of the image. Solid lines and circles are for DOY 14 (Australian summer) and dash lines and circles are for DOY 190 (Australian winter).

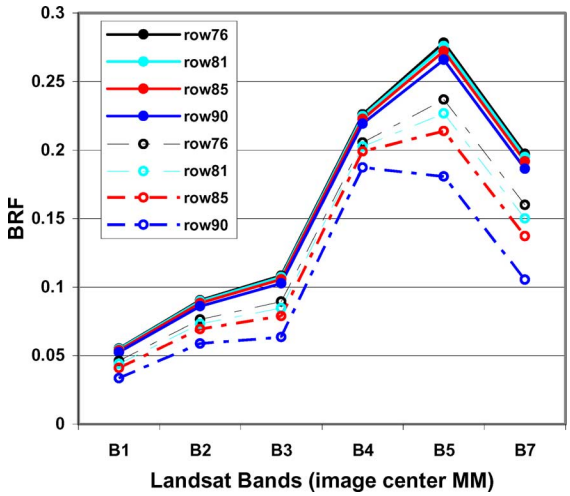

Fig. 4. BRF at center of the image (MM) varies with seasons and geographical locations. Symbols correspond to Landsat row numbers. Solid lines and circles are for DOY 14 (Australian summer) and dash lines and circles are for DOY 190 (Australian winter).

northern South Australia (center location 30.78S, 139.68E). The Gwydir campaign was conducted from the 24th to the 26th of June 2008. A Landsat 7 image was acquired on June 23 one day prior to the start of field work. The Lake Frome experiment was undertaken between February 9 and 14, 2009. A Landsat 7 overpass occurred on February 12, 2009. Just prior to the field experiment, a Landsat 5 image was acquired on February 4.

The land surface types at the two experimental sites were completely different in spectral reflectance, brightness and BRDF effect. At the Gwydir site, the emphasis was on collecting bare soil and non-woody vegetation targets because the complex array of measurements required in order to characterize vegetation properties, and particularly those of woody vegetation, was beyond the scope of the field work. Additional emphasis was given to large uniform targets that could be directly compared with the Landsat 7 ETM^{+} data. Seven bare soil and recently planted crops targets were selected. On the other hand, Lake Frome is a dry salt lake with a useful range of conditions of brightness and signature and with large uniform areas of very bright, near white surface in the visible region. Since there is little temporal and spatial variation and the surface is flat, relatively uniform and fine textured, Lake Frome has been used for many calibration studies and it is a good site to validate the outputs of the algorithm. The loess soils in the vicinity can also be used to provide targets that are bright in the shortwave infrared and have reference spectral features. Ten targets at Lake Frome, ranging in brightness from dark to bright and with different reflectance spectra, were selected to measure the reflectance. Fig. 5 shows selected targets marked

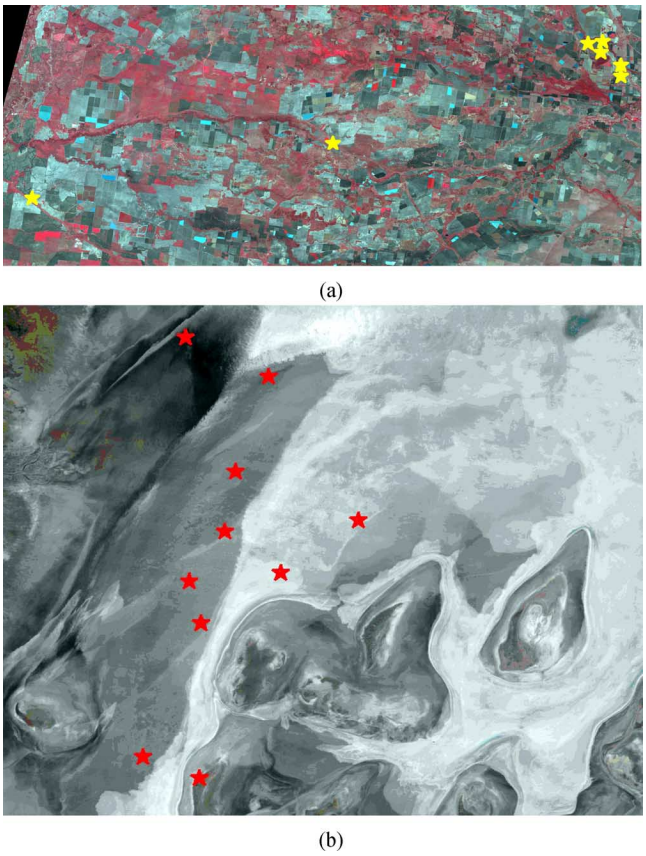

(a)

(b)

Fig. 5. False color images with sampling sites marked: (a) Gwydir field measurement and (b) Lake Frome field measurements.

for Gwydir and Lake Frome respectively on Landsat 7 and 5 false color images.

The spectral reflectance of the various validation targets was measured in the field using a visible-short wave infrared spectroradiometer (ASD-Fieldspec®FR, referred to as ASD in the following and in corresponding figures). In the Gwydir field work, the ASD was held by hand and operated in radiance mode with a 5° field of view and nadir view of the target. A white barium sulphate reference panel was measured at every point. Upwelling radiance measurements were converted to reflectance measurements by dividing the upwelling radiance of the target by the upwelling radiance measured from a barium sulphate field reference panel. Every spectrum was an average of 25 internal measurements recorded by the ASD and at least two spectra were recorded for each target. GPS locations were recorded for each of the spectral averages so that field spectra could be directly compared with the corresponding Landsat pixel. A k-factor correction between the barium sulphate white reference panel and a laboratory reference Spectralon ™ panel was calculated by laboratory staff at CSIRO Land and Water, and this k-factor correction (panel reflectance) was applied to all field spectra.

In the Lake Frome field experiment, where large distances between sites needed to be traversed, the procedure was similar to that of the Gwydir field experiment except that the (same) ASD was mounted on a quad-bike and driven from point to point to cover a 100 m by 100 m square at each site. Regular panel readings were taken to allow for changing irradiance. Lake Frome generally has a wide range of surfaces but variation at a single site was small and the salt surface condition was uniform so that the sampling was kept to a sparse spatial pattern with sufficient internal averaging (in this case 50 samples) for stability. A GPS on the quad-bike was used to measure latitude and longitude for every measurement.

Following the field visits, the ASD data were processed to reflectance factors and converted to Landsat band passes (Fig. 2) numerically. The diffuse radiation was removed from ASD measurements to obtain comparable BRF values using near-surface versions of the expressions derived in Section II. The data were normalized to a 45° solar angle using the parameters of the MODIS BRDF models described next and compared with the data obtained by image processing and atmospheric correction.

2) BRDF Models for Gwydir and Lake Frome: The MODIS BRDF model product [13] is the result of obtaining atmospherically corrected MODIS data over 16 days during which time it is possible to sample directional reflectance for a range of view angles at each location with view zenith angles in the range from $-60°$ to $+60°$. A combination of the Ross Thick volume kernel and the Li-sparse reciprocal [13] geometric kernel models is used to approximate these data.

The development of a statistical BRDF theory [8], [9] has suggested that at an appropriate scale the BRDF should be reciprocal. In our work, following from these developments, we have considered both regional and local effects in MSVA variations. By a "regional" BRDF, we mean the average over a class of some land stratification. The stratification can be by a land cover type, from an area larger than a whole Landsat scene or in wider applications comprise a general surface such as the moon and is at a scale where it is reciprocal. On the other hand, a local MVSA effect is often not reciprocal and can be caused by terrain effects, specific geometric combinations on the ground etc. The difference in spatial resolution between the MODIS (500-m resolution) and Landsat data (30-m resolution) means that the MODIS BRDF product is an appropriate source of data for regional BRDF. Due to subpixel cloud, nonoptimum sampling of the sun and view angles over the compositing period and other effects, the MODIS BRDF model product may be poorly resolved at the pixel scale [22] and since the BRDF model parameters are derived from a statistical fitting method, local variance may be high. These considerations have led many researchers to seek regional strata over which the MODIS BRDF model for BRF or other reflectance factors may be taken to be reciprocal and stable.

Recent work by a number of researchers ([11], [23]–[28]) has found that the BRDF shape function can be linked with land cover types. If such land cover linked data are available, the regional BRDF could be averaged over such land cover types. However, a number of researchers have also experienced the situation where traditional land cover strata are not very effective for stratifying BRDF effect and the interplay of scale and variance may lead to different structural strata being appropriate for POLDER, Landsat and MODIS [12]. Because no final land cover stratification is yet available for this work and because empirical modeling such as that carried out by [10] has shown how effective regional models can be for overcoming the major scene brightening effects in Australian Landsat

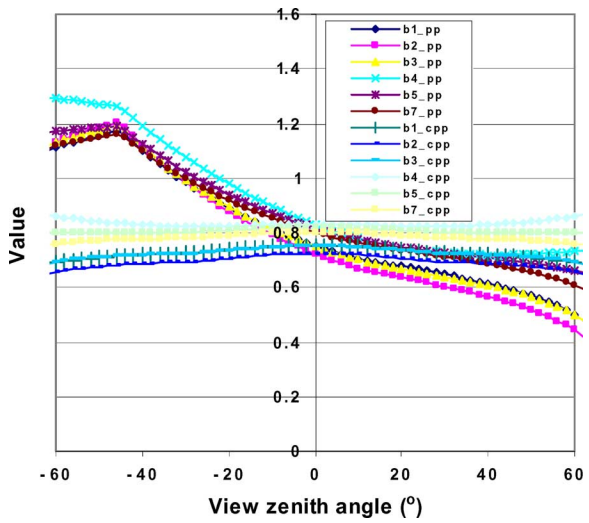

Fig. 6. Regional BRDF BASE shape for Gwydir region where pp is principal plane and cpp is cross principal plane.

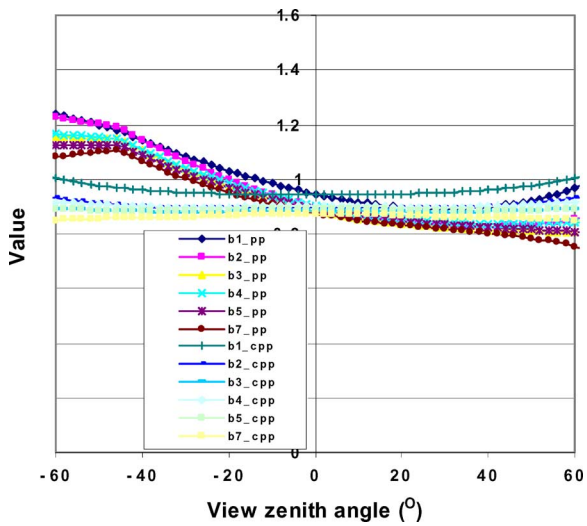

Fig. 7. Regional BRDF BASE shape for Lake Frome region where pp is principal plane and cpp is cross principal plane.

scenes, we have sought to apply a single average BRDF shape function for the Landsat scenes used in our work. These have been simply computed as the average of the coefficients of the MODIS BRDF model product over a region containing the scene to get a regional BRDF shape function. However, in the future, when appropriate land cover data are available, the BRDF shape is planned to be a robust average according to the land cover types.

Fig. 6 shows the Principal Plane and Cross Principal Plane BASE (normalized) BRDF models used for the Gwydir region. The reflectance values in this region are low but BRDF anisotropy is apparent in the shape data. The small amplitude in the BASE in the principal plane is possibly due to lack of measurements in the principal plane available from the MODIS data. A number of researchers have suggested that there is generally more anisotropy in the Principal Plane than is captured in MODIS BRDF model parameters. However, this regional shape function has a level of stability that some individual pixels may not. The BRDF shape function for a region containing Lake Frome in Fig. 7 does show significant anisotropy.

3) Landsat Data Processing: Currently, ortho-corrected images are the standard product for Geoscience Australia and other remote sensing agencies. For an operational method, it is particularly important to be able to work with ortho-corrected images or images in any one of a variety of projections. In this way, the standard processing for atmospheric correction and BRDF normalization will simply add an additional step to the established processing stream and not require it to be modified or disrupted.

For an ortho-corrected Landsat image with latitude and longitude projection, it is more difficult to calculate the satellite view and azimuth angles due to the rotation of the image from the original geometry if no view angle information is provided with the raw data. However, if we assume that the satellite has a circular orbit, the view angle and time (or original image line and, hence, sun position) can be obtained using the model described by [29] if the location of a central pixel on the sub-satellite track is known. Due to the small range of view angles (-7.5° to 7.5°) of the Landsat sensor, if the correction is confined to a single scene, it is possible to simplify the calculations to conveniently compute these positions in the original orbital geometry. Other projections can be handled in a similar way.

In order to minimize the error due to the input environmental data, water vapour and aerosol data were based on measurements made close to the time and location of the image acquisition. The atmospheric profiles of pressure, temperature and water vapour needed for atmospheric correction were obtained from nearby meteorological stations. For the Gwydir field campaign, radiosonde data were obtained from Moree (29.50S, 149.83 E), and Woomera (31.13S, 136.82E) was used for the Lake Frome field experiment. Aerosol data for the Lake Frome field experiment were obtained from the Tinga Tingana Aeronet (-28.976S, 139.991E, see http://aeronet.gsfc.nasa.gov) sunphotometer site. Tinga Tingana is about 100 km north of Lake Frome in a similar atmospheric region. The optical depths at 550 μm were 0.1297 and 0.0978 for February 4 and 12, respectively. Since the Gwydir region does not have a nearby sunphotometer station, aerosol optical depth was based on a combination of visibility estimates, image dark values and the visibility estimated by FLAASH software [21] using the DDV (dense dark vegetation) method. The optical depth for June 23, 2008 was estimated to be 0.083. BRDF shape functions were derived from NASA sixteen day composite MODIS BRDF model products (https://wist.echo.nasa.gov/api/).

In the future, Global Data Assimilation System (GDAS) data will be used for the atmospheric profile to replace the radiosonde measurements for the operational process. Aerosol data will be the combination of look up table, dark dense vegetation (DDV) and other methods. How these data work and how they affect the accuracy of the product will be reported in the future.

4) Algorithm Validation: Fig. 8 compares the corrected field ASD reflectance factor measurements (BRF) resampled to Landsat bands and the retrieved Landsat 5 and 7 BRF data. Both ASD and Landsat BRF were normalized to the same view and solar angles (present nadir view and 45° solar angle) using the (regional) BRDF model selected for image processing. The figure shows that the results are generally good with root

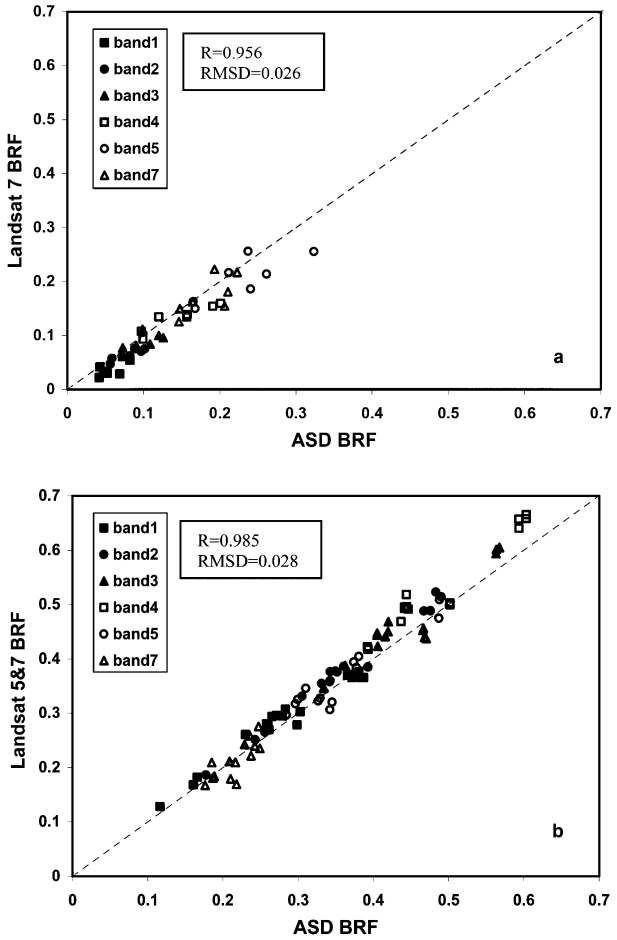

Fig. 8. Comparison between processed ASD diffuse corrected and normalized BRF and BRDF and atmospheric corrected BRF from Landsat 5 and 7: (a) Gwydir field measurement and (b) Lake Frome field measurements. Dashed line represents perfect agreement.

mean square difference (RMSD) for both sites being less than 0.028 (reflectance units) and R values both above 0.950. The data for all sites and all bands are combined in these data sets and include positioning, data collection and other unavoidable sources of variation. For the Gwydir area, the BRF values retrieved from Landsat are slightly lower than those from the ground measurements [Fig. 8(a)]. It is partly due to the fact that the image was acquired during the Australian winter with a low solar angle when the signal/noise ratio is low. In this situation, some areas can generate lower signals due to specific shadow effects etc. A BRDF shape function is generally not able to account for these effects which are often not reciprocal. For the Lake Frome measurements, the situation was better since the experiment was conducted during the summer [Fig. 8(b)]. Both Landsat 5 and 7 result in good agreement with ground measurements except for band 4 where Landsat BRF values were generally higher than the ASD values.

If no BRDF correction were conducted, such as the product from FLAASH [21], the RMSD deteriorated slightly with RMSD just above 0.031 reflectance values for both sites when they are compared with the ASD measurements. It has to be pointed out, however, that the field reflectance measurements in this case were only used to validate the combined effects of BRDF and atmospheric correction. It is difficult to validate BRDF correction separately using such field measurements since they are often obtained at times close to a satellite overpass and at measuring sites with near nadir view. For example, both Gwydir and Lake Frome are located within 3° view angles at the satellite. The difference between correction using "center point" correction and the algorithm proposed here was only 0.003 reflectance values. Nevertheless, the level of agreement achieved, given the differences in spatial scale, are encouraging for the production of a standard reflectance product and removing BRDF effects due to DOY is still essential in these areas of relatively low anisotropy due to the variation (0.09 reflectance values for some wavelengths) created by seasonal BRDF effects (Figs. 3 and 4) even at these latitudes.

B. BRDF Validation Using Image Overlap Areas

An image overlap area is one covered by two adjacent paths imaged within a relatively short time period. The shortest time that can be achieved is 7 days but in practice it will usually be longer. If no rainfall occurs between the two satellite overpasses and the ground vegetation is not fast growing, the reflectance properties of the area can be assumed the same. However, because the area is located in different parts of the two images for the adjacent paths, that is, the western edge of the image for one path and the eastern edge of the image for the other path, the retrieved reflectance factor may be different if no MSVA correction is conducted. Therefore, an overlap area provides a good opportunity to observe BRDF effects and validate BRDF correction. It also has the additional practical benefit of evaluating whether physically based methods can be used to create effective mosaics without empirical adjustment.

After examining land cover and weather conditions, paths 95 and 96 and row 75 of November, 2006 were selected. Path 95 was obtained on November 13, 2006 and Path 96 was obtained on November 20, 2006. Two small uniform targets were selected in the image overlap area. For target 1, the center latitude is 20.902°S and 144.761°E. It is around 16×19 km and located on the upper left for Path 95, but the upper right for Path 96. The central geographical location for target 2 is 22.238°S and 144.471°E. It is around 12×14 km and located lower left for Path 95 and lower right for Path 96. The images are located to the north of the Tropic of Capricorn. The processing procedure was as same as described in previous sections. Input data, such as water vapour and aerosol were selected using nearby stations. Fig. 9(a) and (b) shows the results of using different processing methods for target 1 and 2 respectively. Both reflectance factor values are the average of the whole areas so that the comparison will minimize error arising from pixel mismatch. The results clearly show that using the BRDF correction algorithm described in the previous sections the normalized reflectance factor from both paths 95 and 96 are very close. However, if a conventional method without BRDF correction is used, the derived reflectance factors from path 95 is 0.010~0.025 units higher than path 96. This results in visible brightening at the left side of image and darkening at the right side of the image when the two uncorrected paths are mosaicked together. Fig. 9 also show that the difference in reflectance factor values between

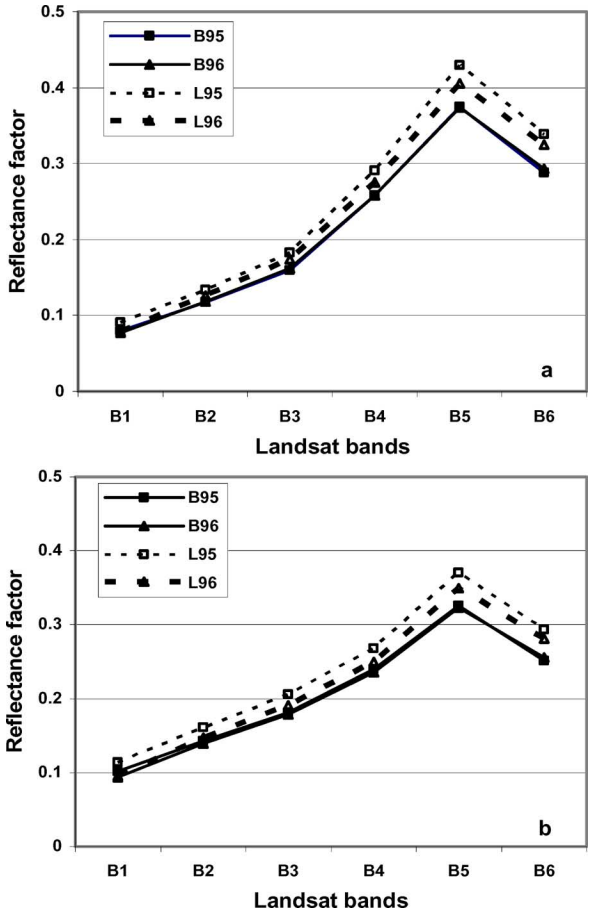

Fig. 9. Reflectance factor products comparison computed from different processing methods for image overlap areas: (a) target 1, (b) target 2. Symbols B95, B96 are reflectance factor with BRDF correction for paths 95 and 96, respectively, whereas L95, L96 is reflectance factor without BRDF correction for paths 95 and 96.

corrected and uncorrected data can be over 0.05 of a reflectance unit.

C. Comparison With MODIS Data

A comparison was also made between the MODIS NBAR product [13] and Landsat data. Since a considerable amount of Landsat 7 data are missing due to the Scan Line Corrector (SLC) failure; it is, therefore, hard to compare with MODIS data on a pixel by pixel basis. Consequently, the Landsat 5 image obtained on February 4, 2009 at Lake Frome site was used. An approximately 50×80 km box was used in which to compare the data sets. The Landsat bands and their associated MODIS bands were as previously described.

Fig. 10 shows the results. In the figure, both MODIS and Landsat TM NBAR (BRF) values were normalized to a 45° solar zenith and zero view angles. The MODIS data are 500 m resolution 16-day composites from January 25 to February 9, 2009. Because the Lake Frome site is relatively uniform and reflectance does not change very much within a month unless rainfall occurs, the two data sets are comparable. For the comparison, Landsat data are aggregated to MODIS resolution. Overall the agreement between MODIS and the Landsat product is good (Fig. 10) with R^2 values ranging between 0.930 and 0.970 in all bands except Landsat Band 5. In most cases, the BRF falls close to the 1:1 line. However, in Landsat band 5 (MODIS band 6), the slope departs from 1 and the R^2 value is 0.900. In general, Landsat band 5 derived NBAR is lower than that for MODIS band 6 data when the BRF is low, but higher than MODIS when BRF is high. In addition, for Landsat band 1 (MODIS band3), the Landsat NBAR is cut off at 0.37 due to sensor saturation in this band. MODIS does not have this problem. The value retrieved from Landsat Band 2 is slightly higher than from MODIS.

For Lake Frome, although it is very uniform on the surface as can be seen in Landsat bands 1–3, the water content underneath the salt is not uniform. This can create a discrepancy between the two sensors, especially in the Near Infrared (Landsat band 4) and Shortwave Infrared (Landsat bands 5 and 7) due to the difference in spatial resolution. It has also been suggested that some discrepancy could be due to the differences between the Landsat and MODIS band passes [30]. As indicated in Fig. 2 and Table I, MODIS bands have a relatively narrow band width (or FWHM) compared with Landsat bands. An analysis of the consequence of this difference has been made by accumulating ASD based measurements to both Landsat and MODIS bands using their response functions for the site data from Lake Frome. Fig. 11 shows the comparison. It should be noted that the band numbers in Fig. 11 are the Landsat bands. The corresponding MODIS bands were provided previously. Fig. 11 has some similarities with Fig. 10 with the BRF for MODIS being lower than Landsat for the green band (Landsat bands 2). For Landsat bands 1, 3, 4, and 7, it seems that both Landsat and MODIS are very close. For Landsat band 5, the reflectance factor from MODIS is often larger than Landsat except when the reflectance factor is high. Unfortunately, there is not enough sampling at the low and high BRF end of the range to show the complete trend. However, in general, Figs. 10 and 11 are consistent.

Taken together, the initial results suggest a physically based model can produce a reflectance product that is comparable and physically consistent with appropriately processed ground based data and also regional scale satellite data such as MODIS. Provided the systematic effects of varying spatial and spectral scale are taken into account, such consistencies allow effective satellite inter-comparison as well as other advantages as previously discussed in Section I that empirical models can not achieve.

V. Conclusion

The investigation reported here has shown that an algorithm which uses MODIS BRDF model shape functions and a relatively fast method based on the MODTRAN radiative transfer model can provide consistent and validated normalized surface reflectance factor products which are relatively free of major regional sun and view angle effects. In particular, it shows how, using the coupled BRDF and atmospheric model developed by the MODIS science team, good estimates of the Landsat normalized surface reflectance factor and the extent of the BRDF effect on Landsat images can be achieved. Such an algorithm could be applied to the large number of images from a variety of satellites that cover and monitor the Australian continent and be consistent with images processed in a similar way for a number

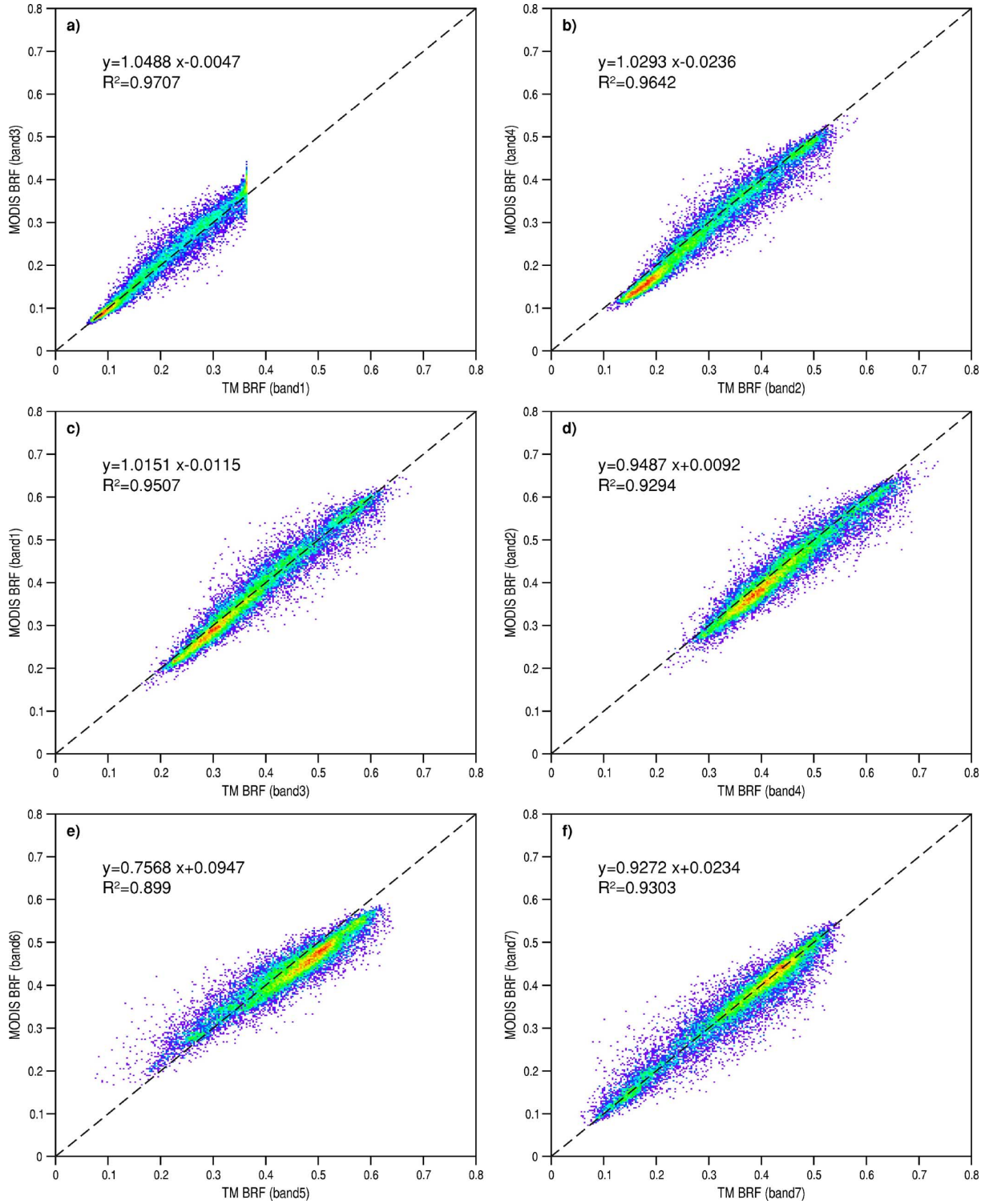

Fig. 10. Comparison between MODIS NBAR (16 days composite) and Landsat TM NBAR product.

of sensors imaging other parts of the world and at different times of the year.

The retrieved Landsat BRF has been shown to be consistent with appropriately processed ground based ASD measurements for two different environments with bare soil and vegetation in the Gwydir area and a dry salt lake at Lake Frome. The statistics show that the RMSD for both areas is less than 0.028 reflectance units. The image overlap analysis conducted on two adjacent paths where significant MSVA effects occur shows that the algorithm can remove most of the BRDF effect and reduce the difference in reflectance values for the two paths from > 0.05 reflectance units to ~ 0 which the a method ignoring the MSVA effect can not. The reflectance factor difference between left and right edges of the images shows that an observable MSVA effect can exist for Landsat images if no BRDF correction is applied.

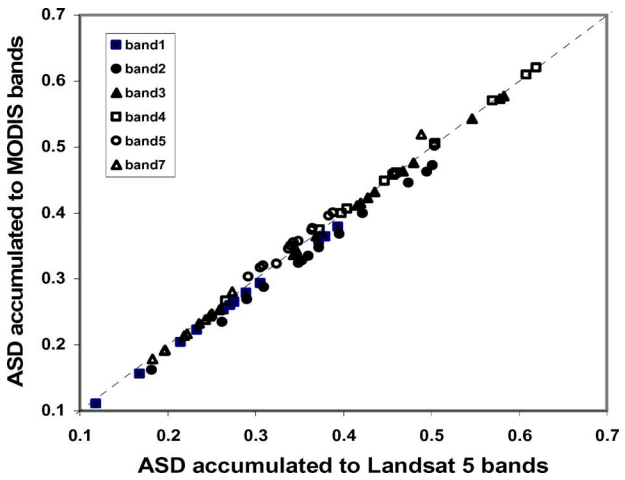

Fig. 11. Comparison of accumulated (resampled) ASD measurement using Landsat and MODIS response function.

The comparison between Landsat and MODIS NBAR when normalized in the same way using the same reflectance factor type shows that there is good relationship between the two products. In the future, this relationship could be used to cross-calibrate and validate between the MODIS NBAR product and a Landsat NBAR product and to link them with airborne and ground based information based on consistent physical reflectance factors. The time series analysis in the east part of Australia (path 91) using a BRDF model shows that although the BRF variation is sometimes not significant for a single Landsat scene, it is always an important factor in seasonal and geographical variations. The absolute reflectance value can vary over 0.09 due to the solar angle variation and spectral differences are common. The BRDF variation over different geographic locations and seasons due to the sun angle change should be addressed and an NBAR product must include a standard sun angle as well as nadir view.

In addition, not every satellite being used has as a small view angle range as Landsat, even for similar resolution, e.g., IRS-P6 AWIFS. Many areas of interest also occur between the tropics where in summer the BRDF effects can be greater due to the alignment of scan direction with the principal plane and have land covers with significant anisotropy. Therefore, even if the range of view angles of Landsat is relatively small and the variation of BRF in a single scene is, therefore, sometimes insignificant it is necessary that its output products be consistent with the processing and normalization being applied to the other data sets with which it is to be compared or combined. The identification of reliable parameters for standard processing could, therefore, lead to significant advantages for operational land cover products using multisensor satellite data.

ACKNOWLEDGMENT

The authors would like to thank Geoscience Australia for the provision of Landsat images. MODIS BRDF model parameters were downloaded from the NASA MODIS website. Sunphotometer data were from the NASA AERONET site and radiosonde data were obtained from NOAA. The Lake Frome field experiment crew, including staff from CSIRO and Geoscience Australia, collected and processed reflectance data at the Lake Frome site, and G. Byrne (CSIRO Land and Water) provided expertise and support for the field data collection in Gwydir field measurement; he and P. Daniels (CSIRO Land and Water) provided support for processing and analysis. C. Smith and L.-w. Wang from Geoscience Australia kindly contributed their time to review the paper. The anonymous reviewers and editors provided constructive comments and valuable suggestions that significantly improved this paper.

REFERENCES

[1] S. Liang, H. Fang, J. T. Morisette, M. Chen, C. J. Shuey, C. L. Walthall, and C. S. T. Daughtry, "Atmospheric correction of Landsat ETM+ and surface imagery. II. Validation and applications," *IEEE Trans. Geosci. Remote Sens.*, vol. 40, pp. 2736–2746, 2002.

[2] S. N. Goward and D. L. Williams, "Landsat and Earth systems science: Development of terrestrial monitoring," *Photogramm. Eng. Remote Sens.*, vol. 63, pp. 887–900, 1997.

[3] C. De Vries, T. Danaher, R. Denham, P. Scarth, and S. Phinn, "An operational radiometric calibration procedure for the Landsat sensors based on pseudo-invariant target sites," *Remote Sens. Environ.*, vol. 107, pp. 414–429, 2007.

[4] F. E. Nicodemus, J. C. Richmond, J. J. Hsia, I. W. Ginsberg, and T. Limperis, *Geometrical Considerations and Nomenclature for Reflectance, NBS Monograph*. Washington, D.C.: National Bureau of Standards, U.S. Department of Commerce, 1977.

[5] J. V. Martonchik, C. J. Bruegge, and A. Strahler, "A review of reflectance nomenclature used in remote sensing," *Remote Sens. Rev.*, vol. 19, pp. 9–20, 2000.

[6] G. Schaepman-Strub, M. E. Schaepman, T. H. Painter, S. Dangel, and J. V. Martonchik, "Reflectance quantities in optical remote sensing—Definitions and case studies," *Remote Sens. Environ.*, vol. 103, pp. 27–42, 2006.

[7] S. Liang and A. Strahler, Eds., "Land surface bi-directional reflectance distribution function (BRDF): Recent advances and future prospects," *Remote Sensing Reviews*, vol. 18, pp. 83–511, 2000, Special Issue.

[8] W. C. Snyder, "Structured surface BRDF reciprocity: Theory and counterexamples," *Appl. Opt.*, vol. 41, pp. 4307–4313, 2002.

[9] L. D. Girolamo, "Generalizing the definition of the bi-directional reflectance distribution function," *Remote Sens. Environ.*, vol. 88, pp. 479–482, 2003.

[10] S. L. Furby and N. A. Campbell, "Calibration images from different dates of "like-value" digital counts," *Remote Sens. Environ.*, vol. 77, pp. 186–196, 2001.

[11] T. Danaher, X. Wu, and N. Campbell, "Bi-directional reflectance distribution function approaches to radiometric calibration of Landsat ETM+ imagery," presented at the IGARSS, Sydney, Australia, Jul. 2001.

[12] C. Bacour and F. M. Breon, "Variability of biome reflectance directional signatures as seen by POLDER," *Remote Sens. Environ.*, vol. 98, pp. 80–95, 2005.

[13] C. Schaaf, F. Gao, A. H. Strahler, W. Lucht, X. Li, T. Tsang, N. C. Strugnell, X. Zhang, Y. Jin, J.–P Muller, P. Lewis, M. Barnsley, P. Hobson, M. Disney, G. Roberts, M. Dunderdale, C. Doll, R. P. d'Entremont, B. Hu, S. Liang, J. L. Privette, and D. Roy, "First operational BRDF, albedo and nadir reflectance products from MODIS," *Remote Sens. Environ.*, vol. 83, pp. 135–148, 2002.

[14] B. Hu, W. Lucht, and A. Strahler, "The interrelationship of atmospheric correction of reflectances and surface BRDF retrieval: A sensitivity study," *IEEE Trans. Geosci. Remote Sens.*, vol. 37, pp. 724–738, 1999.

[15] E. Vermote, N. El Saleous, C. O. Justice, Y. J. Kaufman, J. Privette, L. Remer, J. Roger, and D. Tanre, "Atmospheric correction of visible to middle-infrared EOS-MODIS data over land surfaces: Background, operational algorithm and validation," *J. Geophys. Res.*, vol. 102, no. D14, pp. 17131–17141, 1997.

[16] E. F. Vermote and A. Vermeulen, Atmospheric Correction Algorithm: Spectral Reflectances (MOD09): Algorithm Technical Background Document 1999.

[17] A. H. Strahler, W. Wanner, C. Schaaf, X. Li, B. Hu, J. Muller, P. Lewis, and M. J. Barnsley, MODIS BRDF/Albedo Product: Algorithm Theoretical Basis Document4.0 ed. 1996.

[18] W. Wanner, X. Li, and A. H. Strahler, "On the derivation of kernels for kernel-driven models of bidirectional reflectance," *J. Geophys. Res.*, vol. 100, pp. 21,077–21,089, 1995.

[19] W. Lucht, C. Schaaf, and A. Strahler, "An algorithm for the retrieval of albedo from space using semiempirical BRDF models," *IEEE Trans. Geosci. Remote Sens.*, vol. 38, pp. 977–998, 2000.
[20] A. H. Strahler, W. Lucht, C. Schaaf, T. Tsang, F. Gao, X. Li, J. Muller, P. Lewis, and M. J. Barnsley, MODIS BRDF/Albedo Product: Algorithm Theoretical Basis Document, 1999 [Online]. Available: http://modis.gsfc.nasa.gov/data/atbd/atbd_mod09.pdf, 5.0
[21] G. W. Felde, G. P. Anderson, S. M. Adler-Golden, M. W. Matthew, and A. Berk, "Analysis of Hyperion Data with the FLAASH Atmospheric Correction Algorithm," presented at the Algorithms and Technologies for Multispectral, Hyperspectral, and Ultraspectral Imagery IX. SPIE Aerosense Conf. Orlando, Apr. 21–25, 2003.
[22] W. Lucht and P. Lewis, "Theoretical noise sensitivity of BRDF and albedo retrieval from the EOS-MODIS and MISR sensors with respect to angular sampling," *Int. J. Remote Sens.*, vol. 21, pp. 81–98, 2000.
[23] A. Wu, Z. Li, and J. Cihlar, "Effects of land cover type and greenness on advanced very high resolution radiometer bidirectional reflectances: Analysis and removal," *J. Geophys. Res.*, vol. 100, pp. 9179–9192, 1995.
[24] D. L. B. Jupp, "Some research and applications in the CSIRO (Australia) Earth Observation Centre on scene brightness due to BRDF," in *Observing Land From Space: Science Customers and Technology*, M. M. Verstraete, M. Menenti, and J. Peltoniemi, Eds. Norwell, MA: Kluwer, 2000, pp. 161–174.
[25] I. F. Grant, "Investigation of the variability of the directional reflectance of Australian land cover types," *Remote Sens. Rev.*, vol. 19, pp. 243–258, 2000.
[26] Y. Luo, A. P. Trishchenko, R. Latifovic, and Z. Li, "Surface bidirectional reflectance and albedo properties derived using a land cover–based approach with Moderate Resolution Imaging Spectroradiometer observations," *J. Geophys. Res.*, vol. 110, no. DOI:10.1029/2004JD004741, p. D01106, 2005.
[27] M. J. Hill, C. Averill, Z. Jiao, C. B. Schaaf, and J. D. Armston, "Relationship of MISR RPV parameters and MODIS BRDF shape indicators to surface vegetation patterns in an Australian tropical savanna," *Canad. J. Remote Sens.*, vol. 34, pp. 247–267, 2008.
[28] E. Vermote, C. O. Justice, and F. M. Breon, "Towards a generalized approach for correlation of the BRDF effect in MODIS directional reflectances," *IEEE Trans. Geosci. Remote Sens.*, vol. 47, pp. 898–908, 2009.
[29] R. B. Forrest, "Simulation of orbital image-sensor geometry," *Photogramm. Eng. Remote Sens.*, vol. 47, pp. 1187–1193, 1981.
[30] S. Liang, H. Fang, M. Chen, C. J. Shuey, C. L. Walthall, C. Daughtry, J. Morisette, C. Schaaf, and A. Strahler, "Validating MODIS land surface reflectance and albedo products: methods and preliminary results," *Remote Sens. Environ.*, vol. 83, pp. 149–162, 2002.

Fuqin Li (M'06–SM'07) received the Ph.D. degree in atmospheric science from Murdoch University, Western Australia, in 2001.

She is currently a Remote Sensing Scientist at the National Earth Observation Group at Geoscience Australia. Her interests are atmospheric and BRDF correction for satellite data, evapotranspiration, and water balance and data assimilation.

David L. B. Jupp received the Ph.D. degree in applied mathematics from Flinders University, South Australia, in 1973.

He is a postretirement Fellow with CSIRO Marine and Atmospheric Research. His interests are in hyperspectral and Lidar remote sensing of vegetation, satellite calibration and validation and physical models for land covers, and imaging. He was formerly Science Leader, CSIRO Earth Observation Centre (EOC). Previous applications have been to Coastal zone (including reefs) and inland waters; thermal data analysis of land surface temperature for soil moisture and water balance. Commercialization has included an early PC-based image processing system, software for airborne spectrometer data, and, more recently, the development of a ground based Lidar system for vegetation mapping.

Shanti Reddy received the Ph.D. degree in thermal infrared remote sensing from Osmania University, India, in 1997.

He is currently a Senior Research Scientist contributing to the National Carbon Accounting System and global carbon monitoring activities at the Department of Climate Change, Australia. Prior to this role, he lead the science team as part of the National Earth Observation Group, Geoscience Australia. His primary interests are in time series analysis of satellite data for land management applications.

Leo Lymburner received the Ph.D. degree in remote sensing of the structure and function of riparian vegetation from the University of Melbourne, Australia, in 2006.

He is currently a Remote Sensing Applications Specialist in the National Earth Observation group at Geoscience Australia. His primary interests are land cover mapping and object oriented image processing with particular interests using multitemporal analysis of medium resolution imagery to characterize fractional cover dynamics and inundation dynamics.

Norman Mueller received the B.A. degree in physics from Macquarie University, Sydney, Australia, in 1995, and the postgraduate diploma in GIS and remote sensing from Charles Sturt University, Australia, in 2008.

He is now a Remote Sensing Applications Specialist in the National Earth Observation group at Geoscience Australia. Before joining Geoscience Australia, he worked as a Remote Sensing Scientist for an environmental consultancy. His primary interests lie in relating natural distributions to biophysical characteristics in the environment, such as species distributions and habitat.

Peter Tan received the B.Sc. (Hon.) degree in computer science from Monash University, Melbourne, Australia, in 2001. He is currently pursuing the Ph.D. degree at the School of Computer Science and Software Engineering, Monash University, Australia.

He is now a Remote Sensing Data Modeller in the National Observation Group at Geoscience Australia (GA). His research interests include machine learning algorithms, statistical modeling methods, and high performance parallel computing. Before joining GA, he was a data modeler in a wide range of research projects in collaboration with academics and scientists from various universities and government agents.

Anisul Islam received the B.Tech. degree in civil engineering in 1985, the M.Tech. degree in environmental science and engineering in 1988 from the Indian Institute of Technology, Bombay, India, and the Ph.D. degree from the Department of Chemical Engineering, University of Queensland, Australia, in 2002.

He is now an Application Officer at the National Earth Observation group, Geoscience Australia. His research interest is in the application of remote sensing on coastal environments. Before joining Geoscience Australia, he was an engineer with a consulting company in Bangladesh and a research fellow with the Chemical Engineering Department, University Queensland, Australia.